The AAPS Journal (2021) 23: 102
https://doi.org/10.1208/s12248-021-00635-4

Commentary

Is It Time to Use Modeling of Cellular Transporter Homeostasis to Inform Drug-Drug Interaction Studies: Theoretical Considerations

Roberto A. Abbiati[1,2] · M. Guillaume Wientjes[1,3] · Jessie L.-S. Au[1,2,3,4]

Received 8 June 2021; accepted 6 August 2021; published online 25 August 2021

Abstract Mathematical modeling has been an important tool in pharmaceutical research for 50 + years and there is increased emphasis over the last decade on using modeling to improve the efficiency and effectiveness of drug development. In an earlier commentary, we applied a multiscale model linking 6 scales (whole body, tumor, vasculature, cell, spatial location, time), together with literature data on nanoparticle and tumor properties, to demonstrate the effects of nanoparticle particles on systemic disposition. The current commentary used a 4-scale model (cell membrane, intracellular organelles, spatial location, time) together with literature data on the intracellular processing of membrane receptors and transporters to demonstrate disruption of transporter homeostasis can lead to drug-drug interaction (DDI) between victim drug (VD) and perpetrator drug (PD), including changes in the area-under-concentration–time-curve of VD in cells that are considered significant by the US Food and Drug Administration (FDA). The model comprised 3 computational components: (a) intracellular transporter homeostasis, (b) pharmacokinetics of extracellular and intracellular VD/PD concentrations, and (c) pharmacodynamics of PD-induced stimulation or inhibition of an intracellular kinetic process. Model-based simulations showed that (a) among the five major endocytic processes, perturbation of transporter internalization or recycling led to the highest incidence and most extensive DDI, with minor DDI for perturbing transporter synthesis and early-to-late endosome and no DDI for perturbing transporter degradation and (b) three experimental conditions (spatial transporter distribution in cells, VD/PD co-incubation time, extracellular PD concentrations) were determinants of DDI detection. We propose modeling is a useful tool for hypothesis generation and for designing experiments to identify potential DDI; its application further aligns with the model-informed drug development paradigm advocated by FDA.

KEY WORDS model-informed drug development · multiscale model · OATP · quantitative pharmacology · transporter homeostasis

INTRODUCTION

Drug-drug interactions (DDI) resulting in unexpected or undesirable adverse effects are a recognized clinical problem (1). DDI can be caused by interactions leading to changes in pharmacokinetics (PK) or pharmacodynamics; clinical PK-DDI can be due to interactions causing inhibition or stimulation of (a) absorption from the extravascular sites (*e.g.*, gastrointestinal tract), (b) protein-binding and distribution, (c) metabolism, and (d) transporter-mediated uptake or excretion (2).

✉ Jessie L.-S. Au
jau@i-qsp.org
[1] Institute of Quantitative Systems Pharmacology, Carlsbad, California 92008, USA
[2] Department of Pharmaceutical Sciences, University of Oklahoma, Oklahoma City, Oklahoma 73117, USA
[3] Optimum Therapeutics LLC, 1815 Aston Ave, Suite 107, Carlsbad, California 92008, USA
[4] Taipei Medical University, Taipei, Taiwan, Republic of China

US Food and Drug Administration (FDA) expresses low confidence on DDI prediction based on *in vitro* membrane transporter inhibition due to a lack of *in vitro-in vivo* extrapolation (3). Two hepatic organic anion transporting polypeptides on the basolateral membranes of hepatocytes (OATP1B1, OATP1B3) mediate the blood-to-liver uptake of multiple clinically important drugs (*e.g.*, statins, antibiotics, antidiabetics, anticancer drugs, cardiac glycosides). Their dysfunction, due to genetic polymorphism or inhibition by other drugs (perpetrator drugs or PD), reduces substrate uptake and metabolism in liver cells and leads to severe adverse events including deaths. Many drugs that are potent OATP inhibitors *in vitro* cause severe side effects *in vivo* when co-administered with statins (4–10).

The field of DDI evaluation has been experiment-centric. Previous *in vitro* DDI investigations have largely focused on competitive inhibition of the transporter function, where a candidate PD is co-incubated with a victim drug (VD), typically with transporter-overexpressing cells, to determine if PD alters VD uptake into cells. For example, the 2012 FDA guidance highlights studying the VD uptake in the linear range; the typical experimental set-up in the DDI research community is 5-min co-incubation of VD and PD (*e.g.*, (11–15)). This set-up is based on the assumption that PD induces DDI *via* competitive inhibition of transporter-mediated uptake of VD. Multiple studies have since shown that this paradigm led to under-predictions (*e.g.*, between antivirals and rosuvastatin), high false-negatives (*e.g.*, mibefradil, sirolimus, everolimus, tacrolimus), and severe/fatal adverse events in patients (*e.g.*, statin-related rhabdomyolysis); the discovery of DDI between mibefradil with multiple drugs resulted in its withdrawal from market (16–25). Some studies have demonstrated schedule-dependent DDI or long-lasting inhibitions by some agents such as cyclosporine A and MRL-A (5, 24). In October 2017, FDA added pre-incubation studies to its recommendation (*i.e.*, incubating the candidate PD with cells for a minimum of 30 min prior to incubation with the VD).

Mathematical modeling has been an important tool in pharmaceutical sciences for 50+years (26). In 2011, the US National Institutes of Health identified quantitative systems pharmacology (QSP) as a potential new approach to drug development and translational medicine (27). FDA, under the 2017 FDA Reauthorization Act, has committed to adopting model-informed drug development (MIDD) to facilitate the decision-making process and address drug development and regulatory questions (28, 29).

Our group has advocated the use of computation to guide therapy development. An example of successful use is the development of an optimized treatment of nonmuscle-invading bladder cancer; this project involved a 14-center phase III trial comparing the then standard-of-care intravesical mitomycin C for bladder cancer with a model-predicted/optimized treatment. These studies showed that the treatment outcome closely align with model-predictions (18.3% increase in 5-year recurrence-free survival *vs.* the predicted 18–20%) (30–34). To our knowledge, this is the first demonstration of using QSP-based modeling to guide the phase III clinical trial design. In an earlier commentary in this journal, we applied a multiscale model linking 6 scales (whole body, tumor, vasculature, cell, spatial location, time), together with literature data on nanoparticle and tumor properties, to demonstrate systemic bioequivalence of cancer nanotechnology products does not equal target site bioequivalence (35). In the current commentary, we used modeling to test if and how perturbation of cellular homeostasis of membrane transporters would lead to $DDI_{significant}$.

There are many examples of cellular homeostasis serving as a regulatory mechanism of membrane transporters/receptors, *e.g.*, transferrin receptor, ATP-binding cassette transporters, organic anion transporters, or OATP (36–40). In some cases, internalization of membrane proteins is triggered by phosphorylation, *e.g.*, activation of protein kinase C causes phosphorylation and endocytosis, blocks the cytosol-to-membrane recycling, and/or alters the function of multiple transporters such as OATPs (1A2, 2B1, 1B1), dopamine transporter, serotonin transporter, multidrug resistance-associated protein 2, and cationic amino acid transporter-1 (41–54). Other perturbations of intracellular trafficking, *e.g.*, enhanced lysosomal degradation and Golgi complex disruption reduce the level and transport function of OATP1A2 and OATP1B1 (52). The homeostasis of OATP1B1 and OATP1B3 and responses to perturbation of intracellular processing are largely unknown.

Based on the above information, we developed a 4-scale model (cell membrane, intracellular organelles, spatial location, time) together with literature data on the intracellular processing of membrane receptors and transporters to demonstrate disruption of cellular transporter homeostasis can lead to $DDI_{significant}$. In this report, spatial location refers to where the object-of-interest (*e.g.*, a drug or transporter) is located within a cell (*e.g.*, cell membrane, endocytic organelles, intracellular components). Model simulations were performed to evaluate the effects of perturbation of five major endocytic processes (*i.e.*, transporter internalization, recycling, synthesis, early-to-late endosome transfer, degradation) and to identify the experimental conditions that would affect DDI detection. Note that there have been several PK models on DDI, with strong focus on drug PK and transporter inhibition (55–59). None of these earlier models deal with the intracellular processing of transporters and hence could not be used to evaluate the effects of their perturbations. The current study provides a theoretical analysis of the effects of perturbations of cellular transporter homeostasis.

METHODS

Overview

The computational model for OATP1B1 and OATP1B3 cellular homeostasis and perturbations comprises three components: (**a**) transporter homeostasis including the endocytic kinetic processes, (**b**) PK of extracellular and intracellular drug concentrations, and (**c**) pharmacodynamics of PD-induced stimulation or inhibition of individual endocytic transfer and intracellular processes. The time-dependent processes were described by ordinary differential equations. $DDI_{significant}$ is defined as having PD-induced changes in C-T curve of VD in cells ($AUC_{VD,cell}$) to < 80% or > 125% of the baseline value without PD. These values were selected in part based on the 2017 FDA Draft Guidance (60) that uses a "default no-effect boundary of 80% to 125%" (61) and in part based on the examples that the hepatic clearance of OATP substrates, including pitavastatin, rosuvastatin, atorvastatin, and fluvastatin, is determined by their uptake into metabolizing cells (62).

Model Structure and Assumptions

Figure 1a shows the model that summarizes the current knowledge of intracellular processing of membrane transporters, including biogenesis, endocytic transport, and processing of membrane proteins in general and OATP proteins in particular (63–66). Briefly, proteins are internalized, *e.g.*, *via* clathrin- or caveolae-mediated endocytosis, and located in early endosomes (EE), a tubule-vacuolar vesicle whose tubular region undergoes recycling *via* recycling endosomes (RE) back to the cell membrane while the vacuolar domain matures into multivesicular bodies (MVB), forming intraluminal vesicles (ILV). MVB are exocytosed *via* exosomes, or mature into late endosomes (LE) and eventually into lysosomes (LYSO) where the endosomal contents are degraded (36, 67–71). For biogenesis, OATP1B1 and OATP1B3 promoters are transactivated by hepatic nuclear factor (HNF) 1α, farnesoid X receptor, or transcription factor Stat5 and repressed by HNF3β; the newly synthesized proteins undergo N-glycosylation in endoplasmic reticulum (ER) and Golgi apparatus, followed by transport to plasma membrane; disruption of OATP1B1 glycosylation leads to retention in ER (65, 66, 72–74).

As VD uptake into cells requires the presence of transporter on the membrane, the model is focused on the spatial distribution of the transporter protein in a cell. The model assumptions were based in part on the above endocytic mechanisms and in part on the knowledge regarding transferrin homeostasis. OATP refers to either OATP1B1 or OATP1B3. The assumptions included (a) rapid OATP

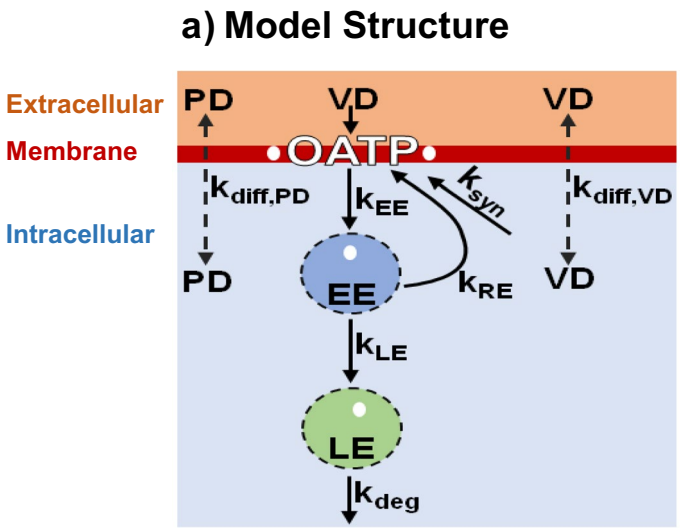

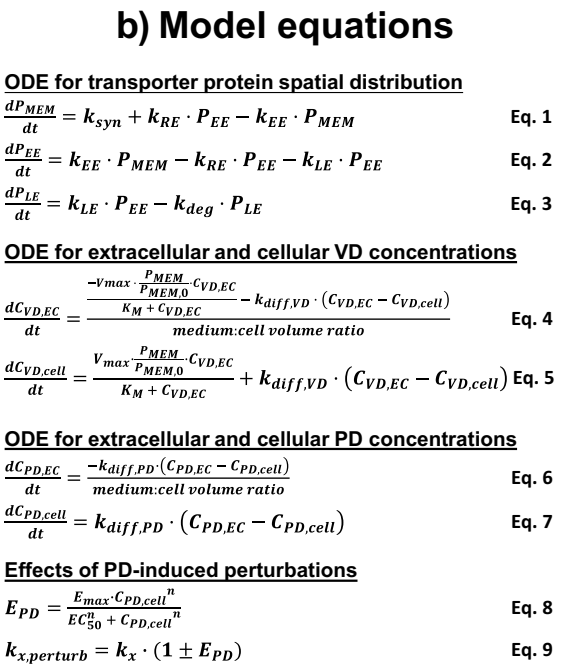

Fig. 1 Model structure, governing equations, and model parameters. **a** Model depicting processes involved in membrane transporter homeostasis (see text). EE, early endosomes; LE, late endosomes; RE, recycling endosomes. Transporter synthesis was zero order whereas all inter-compartmental transfer kinetic processes were first order. **b** Governing ordinary differential equations (ODE, see text). P_{MEM} is membrane transporter at time t and $P_{MEM,0}$ is at the baseline value without PD perturbation. All other parameters are denoted in the table

recycling to membrane, (b) degradation of OATP in LE/LYSO, (c) zero-order OATP biosynthesis (75–77) at a slower rate relative to other processes; this is based on the finding that ~ 25% of total liver protein is synthesized over 24 h (78) and the finding of no detectable changes in the OATP levels in cell membrane in the absence or presence of a protein synthesis inhibitor cycloheximide after 120 min (43), (d) all other inter-compartmental transfer kinetic processes are first order, (e) the transporter is distributed mainly in membrane, EE, and LE with negligible amounts in other cellular locations (*e.g.*, cytoplasm), (f) OATP substrates enter a cell primarily by OATP-mediated transport and to a minor extent by passive diffusion, *e.g.*, studies in hepatocytes have shown that ~ 80% transporter-mediated uptake for pitavastatin (79, 80), (g) VD exits cells *via* passive diffusion, (h) non-OATP substrate PD enters or exits cells *via* passive diffusion and affects only the intracellular processes without competing for transporter-mediated uptake, (i) PD reversibly stimulates or inhibits selected intracellular processes as function of the intracellular PD concentrations, (j) negligible exocytosis of OATP (*i.e.*, OATP is not sorted into MVB, ILV, or exosomes), (k) no significant metabolism or elimination of VD or PD in the cell over the 1-h *in vitro* incubation, (l) the total amount of cellular OATP at baseline (in the absence of PD) is constant and its lysosomal degradation is offset by *de novo* protein synthesis (81), and (m) only the free (*i.e.*, not macromolecule-bound) PD is pharmacologically active.

Governing Equations

Equations for the above spatiotemporal processes are shown in Fig. 1b. Subscripts are used to denote the location of transporter protein (*e.g.*, P_{MEM} is protein located on the membrane) and the location of VD or PD (*e.g.*, $C_{VD,EC}$ is concentration of VD in extracellular fluid and $C_{PD,cell}$ is concentration of PD in intracellular space). Equations 1–3 describe the cellular homeostasis of a transporter, including the time-dependent changes in its levels in cell membrane and endocytic organelles, due to synthesis (with k_{syn} as the rate constant), endocytosis (k_{EE}), recycling (k_{RE}), transfer from EE to LE (k_{LE}), and degradation in LE/LYSO (k_{deg}). Equations 4–5 describe the time-dependent changes in $C_{VD,EC}$ and $C_{VD,cell}$ due to the saturable transporter-mediated uptake and passive diffusion across the cell membrane of VD and the PD-induced perturbations in transporter homeostasis. The saturable transport of VD is described by Michaelis–Menten kinetics where V_{max} is the maximal uptake rate and K_M is the VD concentration at 50% V_{max}. Equations 6–7 describe the time-dependent changes in $C_{PD,EC}$ and $C_{PD,cell}$ including the transport of PD into cells via passive diffusion. Equations 8–9 describe the pharmacodynamics of PD-induced perturbations (stimulation or inhibition) of individual intracellular trafficking processes as function of $C_{PD,cell}$, where EC_{50} is $C_{PD,cell}$ that produces 50% of the maximum effect E_{max} and n is the Hill coefficient.

Model Parameterization

Table I summarizes the model parameters and their values. The total amount of OATP in a cell was arbitrarily assigned as 100 units, with an initial distribution ratio on cell membrane, EE, and LE (MEM:EE:LE ratio) of 80:18:2. This ratio was selected based on the previous finding of a 85:15 membrane:intracellular ratio for OATP2B1 in MDCKII cells (37) and the semi-quantitative microscopic results showing the substantially higher membrane levels of several OATP transporters *vs.* intracellular levels (*e.g.*, OATP2B1 in Caco-2 cells and OATP1B1 and OATP1B3 in HEK293 cells (82, 83).

For the rate constants, k_{EE} was set at 0.1 min^{-1} based on the time (10 min) required for transfer from cell membrane to EE (84). Selection of a suitable k_{LE} value was more difficult due to the less definitive literature data. One report indicated a 15–40-min lag time for the endocytosed cargo to appear in LE (84). Another showed that > 99% of the internalized transferrin is recycled to the membrane with < 1% entering and degraded in LE in 2 h (43). A third report showed no detectable OAT1 in LYSO after 45 min (43). We chose a value of 0.0067 min^{-1}, which is the logarithmic mean of 0.001 min^{-1} (corresponding to < 5% entering LE as observed for transferrin) and 0.025 min^{-1} (corresponding to a 40-min lag time). The selection of $k_{diff,VD}$ value was guided by the kinetic data of intracellular accumulation of drugs in HEK293 cells; these drugs showed a wide range of intracellular-to-extracellular ratios (from ~ 1 to > 300) (85). We selected a $k_{diff,VD}$ value of 0.08 min^{-1} which satisfied the following two boundaries: (a) yielded a maximal intracellular-to-extracellular ratio of ~ 123 that is in-between the ratio of ~ 50 for simvastatin and ~ 210 for lovastatin and (b) yielded a half-time of 8.7 min to reach 50% of this maximal ratio, which is in-between the half-times for drugs that are or are not substrates of membrane transporters (*e.g.*, 1–2 min for the two statins and > 15 min for a lipophilic agent not known to be a transporter substrate) (85). Transport of small molecule drugs across the cell membrane is usually rapid and occurs in min (86); the $k_{diff,PD}$ was assigned a value of 0.4 min^{-1} (13). The value of k_{syn} was estimated from the turn-over rate of 4000–6000 intracellular proteins, with half-lives ranging from 10 to > 1000 h (87). Using the 10-h half-life, the steady state condition at homeostasis (*i.e.*, rate of synthesis equals rate of degradation), and a zero-order synthesis, we calculated k_{syn} to be 0.12 units*min^{-1}; this value was identical to the value calculated as $k_{LE} * P_{EE}/P_{LE}$ at homeostasis (see below). The rate constants for the remaining three processes (k_{RE}, k_{deg}, k_{syn}), because the intracellular processes are linked to each other, were calculated for

Table I Model Parameter Values and Sources

k_{EE}, rate constant of transporter internalization into EE	0.1 min^{-1}, calculated using literature data (see "METHODS" section)
k_{LE}, rate constant of transporter transfer from EE to LE	0.0067 min^{-1}, calculated using literature data (see "METHODS" section)
k_{RE}, rate constant of transporter recycling to membrane	Calculated as $(k_{EE} * P_{MEM} - k_{LE} * P_{EE})/P_{EE}$ at homeostasis (*e.g.*, 0.438 min^{-1} for MEM:EE:LE of 80:18:2)
k_{syn}, rate constant of transporter biosynthesis	Calculated as $k_{deg} * P_{LE}$ (*e.g.*, 0.12 unit*min^{-1} for 80:18:2 MEM:EE:LE, also equals to the value calculated based on a half-life of 10 h (67))
k_{deg}, rate constant of transporter degradation	Calculated as $k_{LE} * P_{EE}/P_{LE}$ at homeostasis (*e.g.*, 0.06 min^{-1} for 80:18:2 MEM:EE:LE)
$k_{diff,PD}$, rate of passive diffusion of PD across cell membrane	0.4 and 10 min^{-1}
$k_{diff,VD}$, rate of passive diffusion of VD across cell membrane	0.08 min^{-1}, calculated using literature data (see "METHODS" section)
K_M, VD concentration for half-maximal transporter-mediated uptake	4 concentration units (assigned)
V_{max}, maximal uptake rate for transporter-mediated VD transport	1000 concentration units-min^{-1} (assigned)
$C_{VD,EC}$, extracellular concentration of VD	100 concentration units at time zero (assigned), calculated with Eq. 4 at later times
$C_{PD,EC}$, extracellular concentration of PD	0.1 to 10 EC_{50}-equivalent at time zero (assigned), calculated with Eq. 6 at later times
$C_{VD,cell}$ and $C_{PD,cell}$, concentration of VD and PD in cells	Calculated with Eqs. 4–7
$k_{x,perturb}$, PD-induced perturbation of a kinetic process	Calculated with $C_{PD,cell}$ and Eqs. 8–9
P_x, amount of transporter protein at location x	100 units distributed in membrane, EE and LE (assigned)
Medium:cell volume for a spherical cell with a 6.5-μm radius (average value for HEK-293) (69, 72), for 150,000 cells in 1 mL of culture medium: 5798	
MEM:EE:LE ratio (spatial distribution of transporter protein at baseline with no PD) was assigned 9 values from 90:8:2 to 20:78:2	

homeostatic conditions (see equations in Fig. 1b); *e.g.*, their respective values were 0.438 min^{-1}, 0.060 min^{-1}, and 0.12 unit-min^{-1} at the baseline MEM:EE:LE ratio of 80:18:2.

Computational Methods

All programming codes, graphical representations, and calculations used the MATLAB language and procedures. Integration of ordinary differential equations was performed using a MATLAB ODE solver (ODE45 or ODE15s). The quantities-of-interest of model simulations are C-T profile of VD in cells, the corresponding $AUC_{VD,cell}$, and the ratio of $AUC_{VD,cell}$ in the absence or presence of PD (*i.e.*, relative AUC or $AUCR_{VD,cell}$). All AUC values were calculated using the trapezoidal rule.

Model Simulations

We used the above model and model parameters to simulate the effects of PD-induced perturbations of transporter endocytosis, cytosol-to-membrane recycling, transfer of transporter from EE to LE/LYSO, and de novo synthesis (*i.e.*, by changing the respective individual rate constants, k_{EE}, k_{RE}, k_{LE}, and k_{syn}). Simulations were performed for (a) 9 initial spatial distribution of transporter proteins (MEM:EE:LE ratios ranging from 90:8:2 to 20:78:2), (b) perturbations of 4 transfer processes (k_{EE}, k_{RE}, k_{LE}, k_{syn}) plus transporter degradation (k_{deg}), and (c) 2 types of PD effects (inhibition or stimulation), (d) varying extents of PD perturbations including 3 values for the Hill's coefficient n (0.5, 1, 2), 5 values of initial $C_{PD,EC}$ (from 0.1 to 10 times the EC_{50}-equivalents), 7 VD-PD co-incubation durations (from 5 to 60 min), and 2 diffusion rates for PD ($k_{diff,PD}$ values of 10 min^{-1} and 0.4 min^{-1}). The co-incubation times included the typical 5-min duration used in the 2012 FDA-recommended *in vitro* investigations of competitive inhibition of OATP-mediated VD uptake and the 30 min pre-incubation duration in the 2017 FDA recommendation. We set E_{max} at 100% for inhibition (*i.e.*, complete inhibition of a process) and 500% for stimulation (*i.e.*, fivefold increase). Note that because the cell volume under *in vitro* conditions was calculated to be ~5,800 times less than the extracellular culture medium volume, there were no significant changes in $C_{PD,EC}$ or $C_{VD,EC}$ over time. The model-simulated $AUCR_{VD,cell}$ outputs were analyzed by a separate algorithm that identified the incidence of $DDI_{significant}$, *i.e.*, when $AUCR_{VD,cell}$ was < 80% or > 125%.

Sensitivity Analysis to Identify the Critical Endocytic Processes

We performed sensitivity analysis to rank order the individual intracellular processes that, when perturbed, had the greatest effects on $C_{VD,cell}$ at time t and the cumulative

AUC from 0 to 60 min. Each rate constant was increased or decreased by 5% (*i.e.*, δ of 0.05) and the sensitivity index (SI_x) was calculated as the difference between the $AUCR_{VD,cell}$ values without and with change in k_x divided by $\delta * k_x$, where k_x is k_{EE}, k_{RE}, k_{LE}, k_{syn}, or k_{deg}. Multiplication of SI_x with baseline k_x divided by the baseline $AUC_{VD,cell}$ without PD yielded the dimensionless SI values.

RESULTS

Evaluation of Model Suitability for Transporter Protein Homeostasis

We first evaluated if the model captured the expected homeostasis (*i.e.*, steady state); this condition was confirmed by the constant protein levels in cell membrane, EE, and LE over time (Fig. 2a). We next evaluated if the model captured the differences in drug uptake by passive diffusion and via transporter; this condition was confirmed by the model-simulated results, *i.e.*, much slower uptake for passive diffusion (*e.g.*, 8 *vs.* 962 concentration unit*min^{-1}) and a much lower contribution of diffusion-mediated uptake to total VD uptake and $C_{VD,cell}$ (~100-fold lower) compared to transporter-mediated uptake (Fig. 2b). The model further captured the diffusion-mediated efflux from cells due to the intracellular-to-extracellular concentration gradient at the later times, to yield a plateau $C_{VD,cell}$ after 15 min.

Model Simulations

We performed a total of 9,303 simulations (63 for control, 840 for comparing PDs with 2 $k_{diff,PD}$ values, and 8,400 for PD-induced perturbations of 5 endocytic transfer rate constants), to examine if and when such perturbations resulted in $DDI_{significant}$. The results indicate PD-induced perturbations of endocytosis and intracellular processing of membrane transporters led to substantially lower or higher $AUCR_{VD,cell}$ and $DDI_{significant}$. Table II shows the overall incidences of $DDI_{significant}$ due to PD-induced perturbations and Table III shows the break-down of the incidences due to changes in individual endocytic transfer processes and biosynthesis of transporters. These simulation results indicate that (a) the rate of PD diffusion into a cell had a relatively minor effect on $AUCR_{VD,cell}$, (b) the overall incidence of $DDI_{significant}$ was 18.7% and all were caused by PD-induced perturbations in 4 intracellular transfer processes with the rank order of $k_{EE} > k_{RE} > k_{syn} > k_{LE}$ and none by k_{deg}, (c) the time to reach the maximum change in $AUCR_{VD,cell}$ depended on the process affected by the PD and was longer for inhibitory PD than for stimulatory PD, and (d) the magnitude of $AUCR_{VD,cell}$ changes caused by PD depended on the cell property (*i.e.*, baseline spatial transporter distribution or MEM:EE:LE ratio), VD-PD co-incubation time, and $C_{PD,EC}$. These findings are discussed below.

Relationship Between Diffusion Rate and Extracellular Concentration of PD on Spatial Transporter Distribution and DDI

We compared two PDs, both inhibited the sorting of EE content to RE (*i.e.*, lowering k_{RE}) but had a 25-fold difference in $k_{diff,PD}$ (0.4 and 10 min^{-1}); the simulations used Hill coefficient *n* of 1 and 80:18:2 MEM:EE:LE ratio. Both PDs reduced the P_{MEM} and increased the P_{EE} and P_{LE} (Fig. 3). A higher $k_{diff,PD}$ led to more rapid $C_{PD,cell}$ increases, *e.g.*, reaching 50% of $C_{PD,EC}$ at 0.07 min for $k_{diff,PD}$ of 10 min^{-1} *vs.* 1.7 min for $k_{diff,PD}$ of 0.4 min^{-1}; the differences were greatest during the first 15 min and diminished at later times (<2% at 60 min). However, the higher $k_{diff,PD}$ only marginally altered the $C_{PD,cell}$ and did not significantly altered the spatial transporter distribution nor $AUCR_{VD,cell}$. In contrast, increasing the $C_{PD,EC}$ from 1 to 10 EC_{50}-equivalents resulted in much greater changes in spatial transporter distribution (from 15% reduction in P_{MEM} after 15-min co-incubation to 55% reduction) and significant reduction of $AUCR_{VD,cell}$ (from no change to <80%).

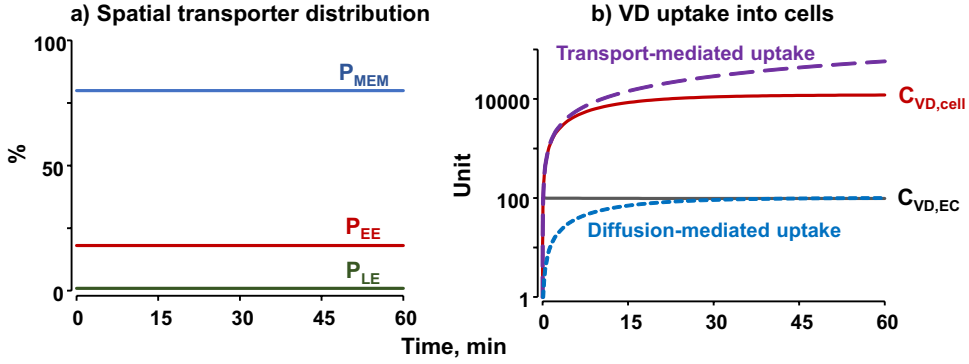

Fig. 2 Evaluation of suitability of model and model parameter values. **a** The plots show apparent steady state levels of transporter proteins in cell membrane (P_{MEM}), EE (P_{EE}), and LE (P_{LE}) and accumulation of $C_{VD,cell}$ over time. **b** Contribution of transporter-mediated uptake and passive diffusion of VD to total $C_{VD,cell}$

Table II Incidence of $DDI_{significant}$ as Functions of Spatial Transporter Distribution and VD-PD Co-incubation Time. Percentages Reflect the Total Incidence of $DDI_{significant}$ Observed in Simulations Using 9 MEM:EE:LE Ratios, 3 n Values (0.5, 1, 2), 5 $C_{PD,EC}$ (0.1, 0.3, 1, 3, and 10 EC_{50}-Equivalents), and 7 VD-PD Co-incubation Times (from 5 to 60 min), as Described in Text. E_{max} for PD-Induced Inhibition Was 100% (*i.e.*, Complete Inhibition of the Process). E_{max} for PD-Induced Stimulation Was 500% (*i.e.*, fivefold Increase Compared to the Baseline Value)

MEM:EE:LE ratio	$AUCR_{VD,cell}$	Incidence of $DDI_{significant}$ at following co-incubation time (min)						
		5	**10**	**15**	**20**	**30**	**45**	**60**
90:8:2	>125%	0%	0%	0%	0%	0%	0%	0%
	<80%	0%	2.50%	5.00%	6.67%	7.50%	7.50%	9.17%
	Total	0%	2.50%	5.00%	6.67%	7.50%	7.50%	9.17%
80:18:2	>125%	0%	0%	0%	0%	0%	0%	0%
	<80%	2.50%	6.67%	9.17%	12.5%	12.5%	13.3%	13.3%
	Total	2.50%	6.67%	9.17%	12.5%	12.5%	13.3%	13.3%
80:10:10	>125%	0%	0%	0%	0%	0%	0%	0%
	<80%	1.67%	5.83%	7.50%	7.50%	10.0%	11.7%	11.7%
	Total	1.67%	5.83%	7.50%	7.50%	10.0%	11.7%	11.7%
70:28:2	>125%	0%	1.67%	3.33%	5.83%	7.50%	11.7%	11.7%
	<80%	5.00%	9.17%	11.7%	12.5%	15.0%	15.0%	16.7%
	Total	5.00%	10.8%	15.0%	18.3%	22.5%	26.7%	28.4%
70:20:10	>125%	0%	0%	0%	0%	0.83%	1.67%	4.17%
	<80%	5.00%	7.50%	11.7%	12.5%	13.3%	14.2%	15.0%
	Total	5.00%	7.50%	11.7%	12.5%	14.1%	15.9%	19.2%
60:38:2	>125%	1.67%	5.00%	8.3%	11.7%	13.3%	14.2%	18.3%
	<80%	5.00%	10.0%	13.3%	15.0%	15.0%	17.5%	17.5%
	Total	6.67%	15.0%	21.6%	26.7%	28.3%	31.7%	35.8%
50:40:10	>125%	2.50%	5.83%	10.8%	12.5%	15.0%	17.5%	22.5%
	<80%	5.00%	10.0%	13.3%	15.0%	15.8%	17.5%	18.3%
	Total	7.5%	15.8%	24.1%	27.5%	30.8%	35.0%	40.8%
30:60:10	>125%	5.00%	8.33%	13.3%	17.5%	22.5%	25.0%	26.7%
	<80%	5.83%	9.17%	14.2%	15.0%	16.7%	17.5%	22.5%
	Total	10.8%	17.5%	27.5%	32.5%	39.2%	42.5%	49.2%
20:78:2	>125%	3.33%	10.8%	18.3%	21.7%	25.8%	26.7%	28.3%
	<80%	5.83%	8.33%	12.5%	14.2%	15.0%	19.2%	24.2%
	Total	9.16%	19.1%	30.8%	35.9%	40.8%	45.9%	52.5%

Table III Contribution of PD-Induced Perturbations in 4 Kinetic Processes to $DDI_{significant}$. Simulations and Calculations of Incidence of $DDI_{significant}$ Are as Described in Table I. The Effects of Individual Perturbations on $AUCR_{VD,cell}$ (>125% or<80%) Are Noted. Neither Inhibition Nor Stimulation of k_{deg} Resulted in $DDI_{significant}$ (Not Shown)

MEM:LE:LE ratio	Incidence of $DDI_{significant}$ ($AUCR_{VD,cell}$ of<80% or>125%) due to PD-induced perturbations							
	k_{EE}		k_{RE}		k_{syn}		k_{LE}	
	Inhibition >125%	Stimulation <80%	Inhibition <80%	Stimulation >125%	Inhibition <80%	Stimulation >125%	Inhibition >125%	Stimulation <80%
90:8:2	0%	3.45%	2.02%	0%	0%	0%	0%	0%
80:18:2	0%	6.90%	3.10%	0%	0%	0%	0%	0%
80:10:10	0%	5.36%	2.62%	0%	0%	0%	0%	0%
70:28:2	1.67%	8.45%	3.69%	4.29%	0%	0%	0%	0%
70:20:10	0.71%	7.98%	3.33%	0.24%	0%	0%	0%	0%
60:38:2	2.86%	8.93%	4.40%	7.02%	0%	0.48%	0%	0%
50:40:10	3.45%	8.93%	4.52%	7.86%	0%	1.07%	0%	0.12%
30:60:10	4.76%	9.29%	4.64%	8.81%	0%	3.33%	0%	0.48%
20:78:2	5.12%	9.52%	3.81%	8.45%	0%	5.71%	0%	0.36%

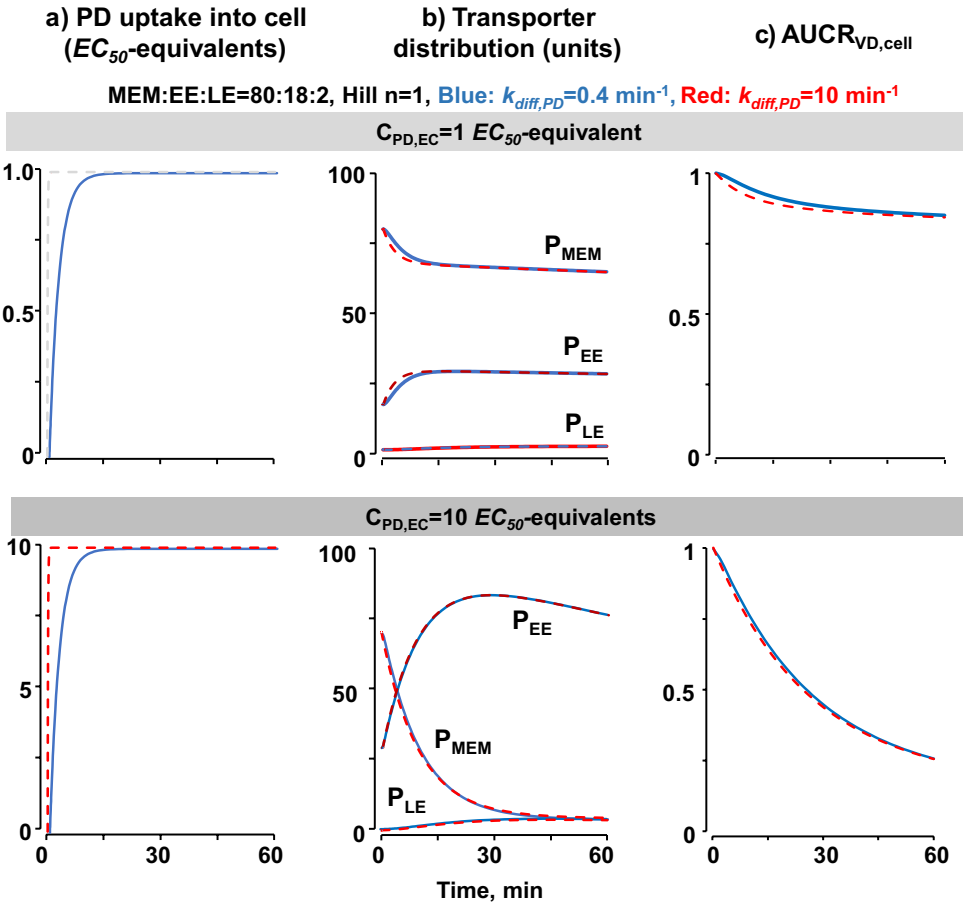

Fig. 3 Effect of PD diffusion rate. Model-based simulation results on the changes of $AUCR_{VD,cell}$ induced by PD with two different diffusion rate constants into cells ($k_{diff,PD}$) of 0.4 min^{-1} (blue) and 10 min^{-1} (red); both PD acted to reduce the transporter transfer from EE to RE (*i.e.*, inhibiting k_{RE}). The plots show the simulation results obtained using the parameter values of n of 1, 80:18:2 MEM:EE:LE ratio, and two initial $C_{PD,EC}$ of 1 EC_{50}-equivalent (top panels) and 10 EC_{50}-equivalents (bottom panels). **a** PD uptake into cell (EC_{50}-equivalents). **b** Transporter distribution. **c** $AUCR_{VD,cell}$

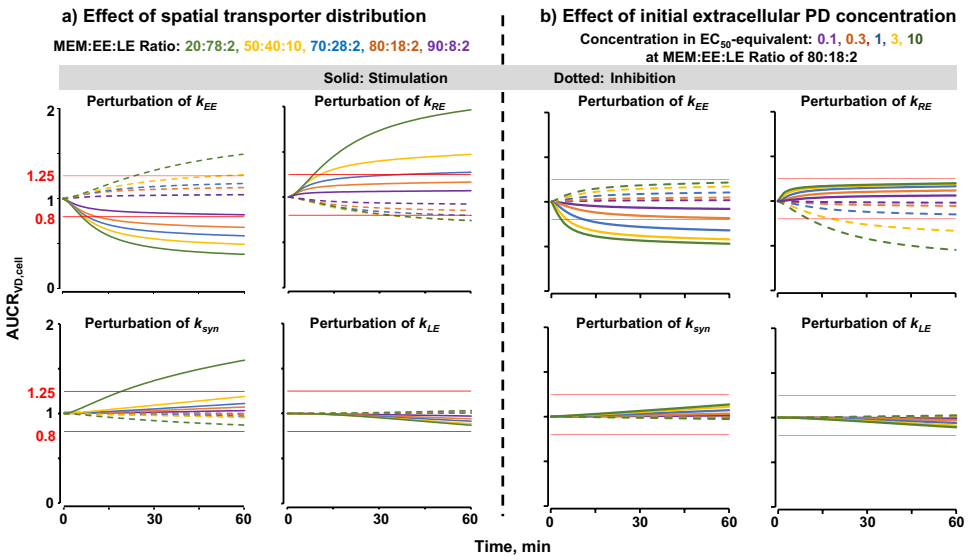

Fig. 4 Effects of spatial transporter distribution and VD-PD co-incubation time. Model-based simulation results on the changes of $AUCR_{VD,cell}$ as functions of PD-induced perturbations in k_{EE}, k_{RE}, k_{syn}, and k_{LE}; spatial transporter distribution (MEM:EE:LE ratio); and co-incubation time. The plots show the simulation results obtained using n of 1. E_{max} for PD-induced inhibition was 100% (*i.e.*, complete inhibition of the process). E_{max} for PD-induced stimulation was 500% (*i.e.*, five-fold increase compared to the baseline value). Solid lines: changes induced by stimulation of respective parameters. Dotted lines: changes induced by inhibition of respective parameters. Red horizon lines indicate $AUCR_{VD,cell}$ of 125% (top) or 80% (bottom). **a** Simulation results obtained at five MEM:EE:LE ratio values, using $C_{PD,EC}$ of 1 EC_{50}-equivalent, to demonstrate the trend and the full range of the changes. **b** Simulation results obtained at one MEM:EE:LE ratio of 80:18:2 and five $C_{PD,EC}$ values of 0.1, 0.3, 1, 3, and 10 EC_{50}-equivalents

Perturbation of Individual Endocytic Processes

Of the five endocytic processes, perturbation of transporter internalization (k_{EE}) or recycling (k_{RE}) led to the greatest $AUCR_{VD,cell}$ changes and the highest incidence of $DDI_{significant}$ (Fig. 4 and Table II). In comparison, inhibition of transporter synthesis (k_{syn}) or EE-to-LE transfer (k_{LE}) did not lead to significant $AUCR_{VD,cell}$ changes and their stimulation led to relatively minor changes under limited circumstances (*e.g.*, high $C_{PD,EC}$ and low P_{MEM}). This is because the changes in P_{MEM}, which determines the VD uptake, are primarily affected by perturbations of k_{EE} and k_{RE} (see Eq. 1–2) due to their higher values (*i.e.*, more rapid processes) compared to the other two processes. For the remaining process of transporter degradation (k_{deg}), neither inhibition nor stimulation resulted in significant $AUCR_{VD,cell}$ changes, as the degraded protein did not re-enter the cell membrane. As summarized below, the stimulation of k_{RE} and k_{syn} and inhibition of k_{EE} and k_{LE} resulted in increased $AUCR_{VD,cell}$ whereas k_{RE}/k_{syn} inhibition and k_{EE}/k_{LE} stimulation resulted in decreased $AUCR_{VD,cell}$. This is because processes that enhance P_{MEM}, such as inhibiting k_{EE} or stimulating k_{RE}, increase VD uptake and $AUCR_{VD,cell}$, whereas processes that reduce P_{MEM} reduce $AUCR_{VD,cell}$.

Stimulation of k_{EE}, which corresponded to enhanced transporter internalization, led to reduced $AUCR_{VD,cell}$. Inhibition of k_{EE} had the opposite effect and increased the $AUCR_{VD,cell}$. In both cases, the magnitude in $AUCR_{VD,cell}$ changes and the incidence of $DDI_{significant}$ depended on the transporter MEM:EE:LE ratio, $C_{PD,EC}$, and VD-PD incubation time (Fig. 4 and Table II). For example, under the conditions of n of 1 and $C_{PD,EC}$ of 1 EC_{50}-equivalent, a change in MEM:EE:LE ratio from 80:18:2 to 20:78:2 caused the $AUCR_{VD,cell}$ to reach the < 80% level at an earlier time (6.31 min *vs.* 11.3 min). Increasing the $C_{PD,EC}$ to 10 EC_{50}-equivalents further increased the incidence and shortened the time to reach DDI. Note that k_{EE} inhibition caused a lower incidence of $DDI_{significant}$ compared to k_{EE} stimulation because (a) the value of maximal stimulation was set at a higher level compared to the maximal inhibition (500% *vs.* 100%) and (b) the effect of k_{EE} inhibition was limited in part by the initial P_{MEM} (*i.e.*, a complete inhibition of k_{EE} would cause all proteins to remain on the membrane, or from the baseline level of 80% to 100%, which equals a relatively small 25% increase).

Stimulation of k_{RE} led to more rapid recycling and reappearance of the endocytosed transporter on cell membrane and elevated the $AUCR_{VD,cell}$, whereas inhibition of k_{RE} yielded opposite effects (Fig. 4 and Table II). As for k_{EE}, changes in $AUCR_{VD,cell}$ and $DDI_{significant}$ depended on MEM:EE:LE ratio, $C_{PD,EC}$, and VD-PD co-incubation time. For example, under the conditions of n of 1 and $C_{PD,EC}$ of 1 EC_{50}-equivalent, $DDI_{significant}$ was reached at an earlier time at the 20:78:2 ratio compared to the 70:28:2 ratio (8.3 min *vs.* 37.9 min), and increasing the $C_{PD,EC}$ to 10 EC_{50}-equivalents increased the incidence and shortened the time to reach DDI. Note the higher incidence of DDI due to k_{RE} inhibition or stimulation when P_{MEM} dropped below 70%.

Inhibition of k_{syn} did not cause $DDI_{significant}$, whereas its stimulation resulted in $AUCR_{VD,cell}$ of > 125%, all of which were observed when P_{MEM} was ≤ 60%.

Inhibition of k_{LE} did not result in $AUCR_{VD,cell}$ of < 80%, whereas its stimulation resulted in a low incidence (up to 0.48%) of $AUCR_{VD,cell}$ of > 125%. Similar to the situation of k_{syn}, all incidences of DDI were observed at low P_{MEM} levels (≤ 50%).

Effects of Experimental Conditions on DDI Detection

We used model simulations to identify three experimental conditions that played a role in detecting PD-induced DDI (Fig. 4, Tables I and II), as follows. First, the frequency and severity of DDI depended on the baseline spatial transporter distribution and generally increased at lower P_{MEM}. For example, the incidence of DDI at 60 min increased by fourfold from ~ 9 to ~ 36% when the membrane transporter decreased from 90 to 60%. Note that only a few situations did not show $AUCR_{VD,cell}$ > 125% irrespective of the changes in k_{EE}, k_{RE}, k_{syn}, or k_{LE} (either stimulation or inhibition), *i.e.*, three situations of ≥ 80% P_{MEM} (MEM:EE:LE ratios of 90:8:2, 80:18:2, and 80:10:10) for k_{EE} or k_{RE} and five situations of ≥ 70% P_{MEM} for k_{syn} or k_{LE}. In contrast, $AUCR_{VD,cell}$ of < 80% or > 125% were observed at all other MEM:EE:LE ratios. Additional simulations showed that the ratio cut-off for $AUCR_{VD,cell}$ to increase to > 125% was 79:19:2 (0.83% incidence at 60 min) whereas the ratio cut-off to decrease $AUCR_{VD,cell}$ to < 80% was 99:0.5:0.5 (0.83% incidence at 20 min).

The second important experimental condition was the initial $C_{PD,EC}$. Figure 4b shows the results obtained for the 80:18:2 MEM:EE:LE ratio. Increasing $C_{PD,EC}$ enhanced the PD-induced perturbations, shortened the time to reach $DDI_{significant}$, and increased the frequency of $DDI_{significant}$. A PD that stimulated a process, by increasing the k value, produced the maximal perturbation more rapidly than a PD that inhibited a process. For example, the change in $AUCR_{VD,cell}$ at $C_{PD,EC}$ of 10 EC_{50}-equivalents reached 50% of the highest level at 4.3 min after stimulation *vs.* 8.2 min after inhibition for k_{EE} and at 2.7 min after stimulation *vs.* 15.2 min after inhibition for $k_{EE.}$.

The third important experimental condition was the VD-PD co-incubation time; increasing the time increased the incidence of $DDI_{significant}$ due to perturbations of k_{EE}, k_{RE}, k_{LE}, or k_{syn}, *e.g.*, the maximum incidence increased from ~ 6% after 5 min to ~ 18% after 15 min, 26% after 30 min, and 28% after 60 min and the average

incidence increased from < 3% at 5 min to > 11% at 30 min and > 14% at 60 min (Table I). Figure 4 shows that the effect of co-incubation time further depended on the spatial transporter distribution in the cell. The maximum incidence of $DDI_{significant}$ increased with time (2.5% at 5 min to 13.3% at 60 min; Table I) at MEM:EE:LE ratio of 80:18:2 and with decreased P_{MEM} (9% at 90% P_{MEM} to 28% at 20% P_{MEM}; Table I) and depended on the homeostasis process that was perturbed (*e.g.*, perturbations of k_{EE} yielded higher incidence of $DDI_{significant}$ compared to perturbations of k_{LE}).

Sensitivity Analysis

Results of sensitivity analysis (Fig. 5) showed that $AUCR_{VD,cell}$ was affected differently by PD-perturbation of k_{EE}, k_{RE}, k_{syn}, and k_{LE}. The SI values generally increased with increasing VD-PD co-incubation time. The overall SI values, calculated for the cumulative $AUCR_{VD,cell}$ over 60 min, (a) showed a rank order of $k_{EE} > k_{RE} > k_{syn} > k_{LE}$ and (b) increased with decreasing P_{MEM}. For example, the SI values for k_{EE} and k_{RE} increased from ~ 0.2 and ~ 0.19 at the 80:18:2 MEM:EE:LE ratio, respectively, to ~ 0.7 and ~ 0.5 at the 20:78:2 ratio.

DISCUSSION

The goal of this commentary is to demonstrate the utility of modeling in the context of MIDD and transporter-mediated DDI. Using the multiscale model, established by integrating the common mathematical approaches and PK tools, and the general knowledge of the intracellular processing of membrane receptor/transporter, we investigated if and how PD-induced perturbation of transporter homeostasis may cause DDI. The model-based simulation results identified at least four intracellular homeostasis processes (transporter internalization, recycling, synthesis, early-to-late endosome transfer) for which PD-induced stimulation or inhibition would lead to $DDI_{significant}$ and at least three experimental conditions that, because they determined the frequency and extent of DDI, require attention. First, the typical 5-min VD-PD co-incubation that has been used to study competitive inhibition of VD uptake would be insufficient to detect the $DDI_{significant}$ caused by perturbations of transporter homeostasis, whereas a 30-min co-incubation, similar to the duration of PD pre-incubation recommended by the 2017 FDA Guidance (60), would be more effective in detecting $DDI_{significant}$. Second, using a higher $C_{PD,EC}$ may shorten the duration of pre- or co-incubation. Third, the fraction of P_{MEM} plays an important role in homeostasis-related DDI, which brings up the need to know (a) if transfecting cells with the

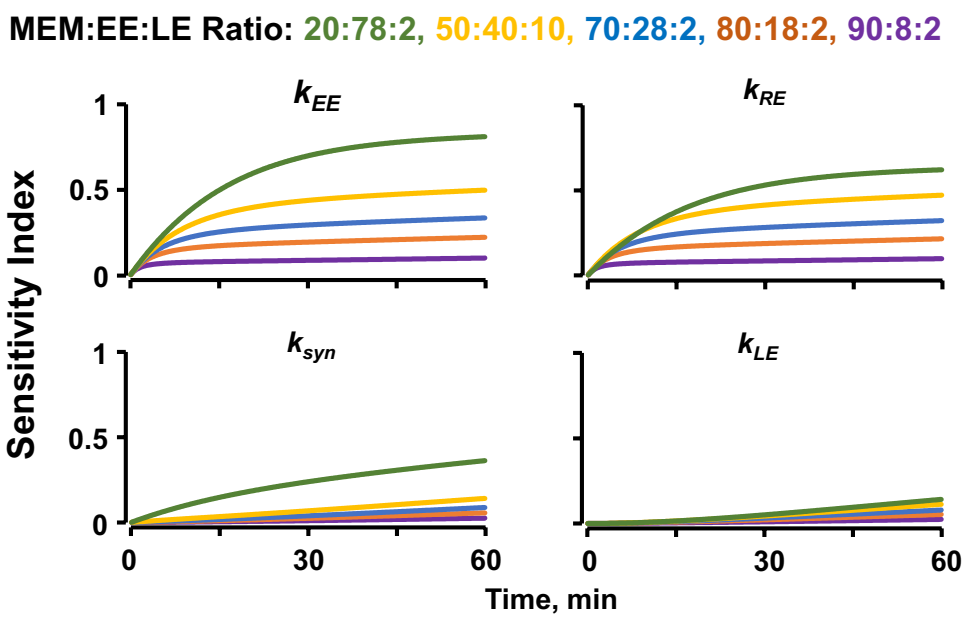

Fig. 5 Sensitivity of $AUCR_{VD,cell}$ to PD-induced perturbations of various kinetic processes. The values of individual rate constants (k_{EE}, k_{RE}, k_{syn}, and k_{LE}) were altered by 5% (increase or decrease) and the resulting changes in $AUCR_{VD,cell}$ were used to calculate the sensitivity indices (SI) as described in text. The plots show the results obtained for δ of + 5% at five MEM:EE:LE ratios, to demonstrate the trend and the full range of the indices; the table shows the SI values calculated for the cumulative $AUCR_{VD,cell}$ over 60 min. Similar results were obtained for δ of − 5% (not shown)

Overall SI values over 60 min at the following MEM:EE:LE Ratios					
Process	**90:8:2**	**80:18:2**	**70:28:2**	**50:40:10**	**20:78:2**
Internalization, k_{EE}	0.091	0.196	0.293	0.428	0.677
Recycling, k_{RE}	0.087	0.188	0.281	0.405	0.515
Synthesis, k_{syn}	0.014	0.031	0.048	0.080	0.251
Transfer from EE to LE, k_{LE}	0.013	0.028	0.040	0.057	0.068

transporter genes alters the spatial transporter distribution and (b) if the DDI identified in the transfected cells reflects the DDI in the parent cells. In view of the importance of DDI in drug development and drug usage, we advocate additional studies to experimentally verify the model simulation results. We further recommend using experimental designs and conditions that, based on the simulation results, are likely to yield the highest incidence of $DDI_{significant}$. These conditions include using cells that are known to have different baseline spatial transporter distribution, high initial $C_{PD,EC}$, and at several VD-PD co-incubation times (*e.g.*, 5 to 60 min).

The current study used 13 model assumptions (see "METHODS" section), including three assumptions derived from previous literature data (OATP biosynthesis, transporter-mediated uptake of OATP substrates, rapid recycling of transporter to membrane), seven assumptions based on the general pharmacological principles or the general knowledge on endocytic processes (*e.g.*, first order intercompartmental transfer, distribution of transporter in endocytic organelles, degradation of transporter in LE/LYSO, transmembrane transport of non-OATP substrates *via* passive diffusion, VD exits cells *via* passive diffusion, concentration-dependent reversible PD effects, only the free PD is pharmacologically active), and two assumptions are based on the absence of contradicting data (negligible exocytosis of OATP, homeostasis of OATP at baseline in the absence of PD). However, the remaining assumption of no significant metabolism or elimination of VD or PD in the cell over the 1-h *in vitro* incubation, which was used mainly to simplify the model, is likely an over-simplification since inhibition of VD uptake into the metabolizing hepatic cells is expected to reduce the VD elimination and hence the DDI. In addition, the current model has not accounted for the potential feedback regulatory processes, *e.g.*, the perturbation of transporter homeostasis may trigger compensatory processes. For refinement, the multiscale model described in Fig. 1 can be adapted to evaluate (a) other treatment schedules such as pre-incubation with PD (*e.g.*, by adding a delayed addition of VD into the extracellular culture medium in the PK computation module), (b) PD-induced perturbations of multiple endocytic processes simultaneously (*e.g.*, weakly basic or lysosomotropic drugs such as chloroquine that, by elevating the pH of multiple endocytic organelles, may affect multiple rate constants including k_{EE}, k_{LE}, or k_{RE}), (c) effects of intracellular drug metabolism (*e.g.*, extend the model to include elimination and effects of inhibitors of lysosomal degradation and intracellular proteasomes), and (d) combinations of drugs that can together perturb multiple intracellular homeostasis simultaneously.

The current study is focused on the effects of perturbations of cellular transporter homeostasis on the cellular PK of VD. On the other hand, the DDI-derived host toxicities are determined by the systemic PK of VD. Additional multiscale modeling studies to link the current, cell-scale model to a whole body-scale model would provide a systems-based approach to depict how the changes in cellular VD concentrations affect the plasma VD concentrations and thereby enable the evaluation of the role of cellular transporter homeostasis in DDI. We propose that modeling is a useful tool for hypothesis generation and for designing experiments to identify potential DDI and that its application aligns with the model-informed drug development paradigm advocated by FDA.

Author Contribution J.L.-S.A. designed the scientific approach, contributed to the interpretation of simulation results, and wrote the manuscript. R.A.A. and M.G.W. formalized and implemented the model, executed simulations, contributed to the interpretation of simulation results, and contributed to manuscript writing.

Funding Supported in part by research grants from NIH (R01CA163015, R01EB015253) and FDA (20919IPAAU, 20919IPAWIENTJES), the Mosier Endowed Chair in Pharmaceutical Sciences at University of Oklahoma Health Sciences Center, and the Chair in Systems Pharmacology at Taipei Medical University.

Declarations

Conflict of Interest The authors declare no competing interests.

References

1. Grymonpre RE, Mitenko PA, Sitar DS, Aoki FY, Montgomery PR. Drug-associated hospital admissions in older medical patients. J Am Geriatr Soc. 1988;36(12):1092–8.
2. Palleria C, Di Paolo A, Giofre C, Caglioti C, Leuzzi G, Siniscalchi A, *et al*. Pharmacokinetic drug-drug interaction and their implication in clinical management. J Res Med Sci. 2013;18(7):601–10.
3. Wagner C, Zhao P, Pan Y, Hsu V, Grillo J, Huang SM, *et al*. Application of physiologically based pharmacokinetic (PBPK) modeling to support dose selection: report of an FDA public workshop on PBPK. CPT Pharmacometrics Syst Pharmacol. 2015;4(4):226–30. https://doi.org/10.1002/psp4.33.
4. Niemi M. Role of OATP transporters in the disposition of drugs. Pharmacogenomics. 2007;8(7):787–802.
5. Tweedie D, Polli JW, Berglund EG, Huang SM, Zhang L, Poirier A, *et al*. Transporter studies in drug development: experience to date and follow-up on decision trees from the International Transporter Consortium. Clin Pharmacol Ther. 2013;94(1):113–25. https://doi.org/10.1038/clpt.2013.77.
6. Shitara Y, Itoh T, Sato H, Li AP, Sugiyama Y. Inhibition of transporter-mediated hepatic uptake as a mechanism for drug-drug interaction between cerivastatin and cyclosporin A. J Pharmacol Exp Ther. 2003;304(2):610–6. https://doi.org/10.1124/jpet.102.041921.
7. Shitara Y, Hirano M, Sato H, Sugiyama Y. Gemfibrozil and its glucuronide inhibit the organic anion transporting polypeptide 2 (OATP2/OATP1B1:SLC21A6)-mediated hepatic uptake and CYP2C8-mediated metabolism of cerivastatin: analysis of

the mechanism of the clinically relevant drug-drug interaction between cerivastatin and gemfibrozil. J Pharmacol Exp Ther. 2004;311(1):228–36. https://doi.org/10.1124/jpet.104.068536.
8. Tirona RG, Leake BF, Wolkoff AW, Kim RB. Human organic anion transporting polypeptide-C (SLC21A6) is a major determinant of rifampin-mediated pregnane X receptor activation. J Pharmacol Exp Ther. 2003;304(1):223–8. https://doi.org/10.1124/jpet.102.043026.
9. Kiser JJ, Gerber JG, Predhomme JA, Wolfe P, Flynn DM, Hoody DW. Drug/drug interaction between lopinavir/ritonavir and rosuvastatin in healthy volunteers. J Acquir Immune Defic Syndr. 2008;47(5):570–8. https://doi.org/10.1097/QAI.0b013e318160a542.
10. Neuvonen PJ, Niemi M, Backman JT. Drug interactions with lipid-lowering drugs: mechanisms and clinical relevance. Clin Pharmacol Ther. 2006;80(6):565–81. https://doi.org/10.1016/j.clpt.2006.09.003.
11. Campbell SD, de Morais SM, Xu JJ. Inhibition of human organic anion transporting polypeptide OATP 1B1 as a mechanism of drug-induced hyperbilirubinemia. Chem Biol Interact. 2004;150(2):179–87. https://doi.org/10.1016/j.cbi.2004.08.008.
12. Umehara K, Iwai M, Adachi Y, Iwatsubo T, Usui T, Kamimura H. Hepatic uptake and excretion of (-)-N-{2-[(R)-3-(6,7-dimethoxy-1,2,3,4-tetrahydroisoquinoline-2-carbonyl)piperidi no]ethyl}-4-fluorobenzamide (YM758), a novel if channel inhibitor, in rats and humans. Drug Metab Dispos. 2008;36(6):1030–8. https://doi.org/10.1124/dmd.108.020669.
13. Karlgren M, Ahlin G, Bergstrom CA, Svensson R, Palm J, Artursson P. In vitro and in silico strategies to identify OATP1B1 inhibitors and predict clinical drug-drug interactions. Pharm Res. 2012;29(2):411–26. https://doi.org/10.1007/s11095-011-0564-9.
14. Izumi S, Nozaki Y, Maeda K, Komori T, Takenaka O, Kusuhara H, *et al*. Investigation of the impact of substrate selection on in vitro organic anion transporting polypeptide 1B1 inhibition profiles for the prediction of drug-drug interactions. Drug Metab Dispos. 2015;43(2):235–47. https://doi.org/10.1124/dmd.114.059105.
15. Vildhede A, Mateus A, Khan EK, Lai Y, Karlgren M, Artursson P, *et al*. Mechanistic modeling of pitavastatin disposition in sandwich-cultured human hepatocytes: a proteomics-informed bottom-up approach. Drug Metab Dispos. 2016;44(4):505–16. https://doi.org/10.1124/dmd.115.066746.
16. Vaidyanathan J, Yoshida K, Arya V, Zhang L. Comparing various in vitro prediction criteria to assess the potential of a new molecular entity to inhibit organic anion transporting polypeptide 1B1. J Clin Pharmacol. 2016;56(Suppl 7):S59–72. https://doi.org/10.1002/jcph.723.
17. Yoshida K, Maeda K, Sugiyama Y. Transporter-mediated drug–drug interactions involving OATP substrates: predictions based on in vitro inhibition studies. Clin Pharmacol Ther. 2012;91(6):1053–64. https://doi.org/10.1038/clpt.2011.351.
18. Yoshikado T, Yoshida K, Kotani N, Nakada T, Asaumi R, Toshimoto K, *et al*. Quantitative analyses of hepatic OATP-mediated interactions between statins and inhibitors using PBPK modeling with a parameter optimization method. Clin Pharmacol Ther. 2016;100(5):513–23. https://doi.org/10.1002/cpt.391.
19. Picard N, Levoir L, Lamoureux F, Yee SW, Giacomini KM, Marquet P. Interaction of sirolimus and everolimus with hepatic and intestinal organic anion-transporting polypeptide transporters. Xenobiotica. 2011;41(9):752–7. https://doi.org/10.3109/00498254.2011.573882.
20. Barshes NR, Goodpastor SE, Goss JA. Sirolimus-atorvastatin drug interaction in the pancreatic islet transplant recipient. Transplantation. 2003;76(11):1649–50. https://doi.org/10.1097/01.TP.0000085287.03333.FC.
21. Hong YA, Kim HD, Jo K, Park YK, Lee J, Sun IO, *et al*. Severe rhabdomyolysis associated with concurrent use of simvastatin and sirolimus after cisplatin-based chemotherapy in a kidney transplant recipient. Exp Clin Transplant. 2014;12(2):152–5. https://doi.org/10.6002/ect.2013.0003.
22. Kotanko P, Kirisits W, Skrabal F. Rhabdomyolysis and acute renal graft impairment in a patient treated with simvastatin, tacrolimus, and fusidic acid. Nephron. 2002;90(2):234–5.
23. Renders L, Haas CS, Liebelt J, Oberbarnscheidt M, Schocklmann HO, Kunzendorf U. Tacrolimus and cerivastatin pharmacokinetics and adverse effects after single and multiple dosing with cerivastatin in renal transplant recipients. Br J Clin Pharmacol. 2003;56(2):214–9.
24. Shebley M, Liu J, Kavetskaia O, Sydor J, de Morais SM, Fischer V, *et al*. Mechanisms and predictions of drug-drug interactions of the hepatitis C virus three direct-acting antiviral regimen: paritaprevir/ritonavir, ombitasvir, and dasabuvir. Drug Metab Dispos. 2017;45(7):755–64. https://doi.org/10.1124/dmd.116.074518.
25. Omar MA, Wilson JP. FDA adverse event reports on statin-associated rhabdomyolysis. Ann Pharmacother. 2002;36(2):288–95. https://doi.org/10.1345/aph.1A289.
26. Wagner JG. History of pharmacokinetics. Pharmacol Ther. 1981;12(3):537–62. https://doi.org/10.1016/0163-7258(81)90097-8.
27. Sorger PK, Allerheiligen SRB, Abernethy DR, Altman RB, Brouwer KLR, Califano A, *et al*. Quantitative and systems pharmacology in the post-genomic era: new approaches to discovering drugs and understanding therapeutic mechanisms. An NIH White Paper by the QSP Workshop Group, 2011. https://www.nigms.nih.gov/training/documents/systemspharmawpsorger2011.pdf. 2011
28. Wang Y, Zhu H, Madabushi R, Liu Q, Huang SM, Zineh I. Model-informed drug development: current US regulatory practice and future considerations. Clin Pharmacol Ther. 2019;105(4):899–911. https://doi.org/10.1002/cpt.1363.
29. Fang L, Kim MJ, Li Z, Wang Y, DiLiberti CE, Au J, *et al*. Model-informed drug development and review for generic products: summary of FDA public workshop. Clin Pharmacol Ther. 2018;104(1):27–30. https://doi.org/10.1002/cpt.1065.
30. Au JL, Badalament RA, Wientjes MG, Young DC, Warner JA, Venema PL, *et al*. Methods to improve efficacy of intravesical mitomycin C: results of a randomized phase III trial. J Natl Cancer Inst. 2001;93(8):597–604.
31. Au JL, Badalament RA, Wientjes MG, Young D, Shen T, Venema PL, *et al*. Optimized intravesical mitomycin C treatment for superficial bladder cancer: long-term follow-up. J Urol. 2006;175(4):268.
32. Gao X, Au JL, Badalament RA, Wientjes MG. Bladder tissue uptake of mitomycin C during intravesical therapy is linear with drug concentration in urine. Clin Cancer Res. 1998;4(1):139–43.
33. Wientjes MG, Badalament RA, Au JL. Use of pharmacologic data and computer simulations to design an efficacy trial of intravesical mitomycin C therapy for superficial bladder cancer. Cancer Chemother Pharmacol. 1993;32(4):255–62.
34. Au JL, Wientjes MG. Intravesical chemotherapy of superficial bladder cancer: optimization and novel agents. In: Lerner SP, Schoenberg MP, Sternberg CN, editors. Textbook of bladder cancer. Taylor & Francis; 2006. p. 341–52.
35. Au JL, Lu Z, Abbiati RA, Wientjes MG. Systemic bioequivalence is unlikely to equal target site bioequivalence for nanotechnology oncologic products. AAPS J. 2019;21(2):24. https://doi.org/10.1208/s12248-019-0296-z.
36. Grant BD, Donaldson JG. Pathways and mechanisms of endocytic recycling. Nat Rev Mol Cell Biol. 2009;10(9):597–608. https://doi.org/10.1038/nrm2755.
37. Zhou F, Lee AC, Krafczyk K, Zhu L, Murray M. Protein kinase C regulates the internalization and function of the human

organic anion transporting polypeptide 1A2. Br J Pharmacol. 2011;162(6):1380–8. https://doi.org/10.1111/j.1476-5381.2010.01144.x.
38. Mayati A, Moreau A, Le Vee M, Stieger B, Denizot C, Parmentier Y, *et al*. Protein kinases C-mediated regulations of drug transporter activity, localization and expression. Int J Mol Sci. 2017;18(4):1–22. https://doi.org/10.3390/ijms18040764.
39. Hong M, Hong W, Ni C, Huang J, Zhou C. Protein kinase C affects the internalization and recycling of organic anion transporting polypeptide 1B1. Biochim Biophys Acta. 2015;1848(10 Pt A):2022–30. https://doi.org/10.1016/j.bbamem.2015.05.011.
40. Takada T, Suzuki H, Gotoh Y, Sugiyama Y. Regulation of the cell surface expression of human BCRP/ABCG2 by the phosphorylation state of Akt in polarized cells. Drug Metab Dispos. 2005;33(7):905–9. https://doi.org/10.1124/dmd.104.003228.
41. Chai J, Cai SY, Liu X, Lian W, Chen S, Zhang L, *et al*. Canalicular membrane MRP2/ABCC2 internalization is determined by Ezrin Thr567 phosphorylation in human obstructive cholestasis. J Hepatol. 2015;63(6):1440–8. https://doi.org/10.1016/j.jhep.2015.07.016.
42. Duan P, Li S, You G. Angiotensin II inhibits activity of human organic anion transporter 3 through activation of protein kinase Calpha: accelerating endocytosis of the transporter. Eur J Pharmacol. 2010;627(1–3):49–55. https://doi.org/10.1016/j.ejphar.2009.10.048.
43. Zhang Q, Hong M, Duan P, Pan Z, Ma J, You G. Organic anion transporter OAT1 undergoes constitutive and protein kinase C-regulated trafficking through a dynamin- and clathrin-dependent pathway. J Biol Chem. 2008;283(47):32570–9. https://doi.org/10.1074/jbc.M800298200.
44. Zhang Q, Pan Z, You G. Regulation of human organic anion transporter 4 by protein kinase C and NHERF-1: altering the endocytosis of the transporter. Pharm Res. 2010;27(4):589–96. https://doi.org/10.1007/s11095-009-9983-2.
45. Zhou F, Hong M, You G. Regulation of human organic anion transporter 4 by progesterone and protein kinase C in human placental BeWo cells. Am J Physiol Endocrinol Metab. 2007;293(1):E57–61. https://doi.org/10.1152/ajpendo.00696.2006.
46. Powell J, Farasyn T, Kock K, Meng X, Pahwa S, Brouwer KL, *et al*. Novel mechanism of impaired function of organic anion-transporting polypeptide 1B3 in human hepatocytes: post-translational regulation of OATP1B3 by protein kinase C activation. Drug Metab Dispos. 2014;42(11):1964–70. https://doi.org/10.1124/dmd.114.056945.
47. Glavy JS, Wu SM, Wang PJ, Orr GA, Wolkoff AW. Down-regulation by extracellular ATP of rat hepatocyte organic anion transport is mediated by serine phosphorylation of OATP1. J Biol Chem. 2000;275(2):1479–84.
48. Hong WC, Amara SG. Differential targeting of the dopamine transporter to recycling or degradative pathways during amphetamine- or PKC-regulated endocytosis in dopamine neurons. FASEB J. 2013;27(8):2995–3007. https://doi.org/10.1096/fj.12-218727.
49. Kock K, Koenen A, Giese B, Fraunholz M, May K, Siegmund W, *et al*. Rapid modulation of the organic anion transporting polypeptide 2B1 (OATP2B1, SLCO2B1) function by protein kinase C-mediated internalization. J Biol Chem. 2010;285(15):11336–47. https://doi.org/10.1074/jbc.M109.056457.
50. Mnie-Filali O, Lau T, Matthaeus F, Abrial E, Delcourte S, El MM, *et al*. Protein kinases alter the allosteric modulation of the serotonin transporter in vivo and in vitro. CNS Neurosci Ther. 2016;22(8):691–9. https://doi.org/10.1111/cns.12562.
51. Rahbek-Clemmensen T, Bay T, Eriksen J, Gether U, Jorgensen TN. The serotonin transporter undergoes constitutive internalization and is primarily sorted to late endosomes and lysosomal degradation. J Biol Chem. 2014;289(33):23004–19. https://doi.org/10.1074/jbc.M113.495754.
52. Sun AQ, Ponamgi VM, Boyer JL, Suchy FJ. Membrane trafficking of the human organic anion-transporting polypeptide C (hOATPC). Pharm Res. 2008;25(2):463–74. https://doi.org/10.1007/s11095-007-9399-9.
53. Vina-Vilaseca A, Bender-Sigel J, Sorkina T, Closs EI, Sorkin A. Protein kinase C-dependent ubiquitination and clathrin-mediated endocytosis of the cationic amino acid transporter CAT-1. J Biol Chem. 2011;286(10):8697–706. https://doi.org/10.1074/jbc.M110.186858.
54. Wu S, Bellve KD, Fogarty KE, Melikian HE. Ack1 is a dopamine transporter endocytic brake that rescues a trafficking-dysregulated ADHD coding variant. Proc Natl Acad Sci U S A. 2015;112(50):15480–5. https://doi.org/10.1073/pnas.1512957112.
55. Taskar KS, Pilla Reddy V, Burt H, Posada MM, Varma M, Zheng M, *et al*. Physiologically-based pharmacokinetic models for evaluating membrane transporter mediated drug-drug interactions: current capabilities, case studies, future opportunities, and recommendations. Clin Pharmacol Ther. 2020;107(5):1082–115. https://doi.org/10.1002/cpt.1693.
56. Wang Q, Zheng M, Leil T. Investigating transporter-mediated drug-drug interactions using a physiologically based pharmacokinetic model of rosuvastatin. CPT Pharmacometrics Syst Pharmacol. 2017;6(4):228–38. https://doi.org/10.1002/psp4.12168.
57. Chen Y, Zhu R, Ma F, Mao J, Chen EC, Choo EF, *et al*. Assessment of OATP transporter-mediated drug-drug interaction using physiologically-based pharmacokinetic (PBPK) modeling - a case example. Biopharm Drug Dispos. 2018;39(9):420–30. https://doi.org/10.1002/bdd.2159.
58. Feng B, Varma MV. Evaluation and quantitative prediction of renal transporter-mediated drug-drug interactions. J Clin Pharmacol. 2016;56(Suppl 7):S110–21. https://doi.org/10.1002/jcph.702.
59. Yang Y, Li P, Zhang Z, Wang Z, Liu L, Liu X. Prediction of cyclosporin-mediated drug interaction using physiologically based pharmacokinetic model characterizing interplay of drug transporters and enzymes. Int J Mol Sci. 2020;21(19):7023. https://doi.org/10.3390/ijms21197023.
60. USFDA. In vitro metabolism- and transporter-mediated drug-drug interaction studies. Guidance for industry. 2017. https://www.fda.gov/media/108130/download.
61. USFDA. Clinical drug interaction studies — study design, data analysis, and clinical implications guidance for industry. 2017. https://www.fda.gov/files/drugs/published/Clinical-Drug-Interaction-Studies-—-Study-Design--Data-Analysis--and-Clinical-Implications-Guidance-for-Industry.pdf.
62. Maeda K. Organic anion transporting polypeptide (OATP)1B1 and OATP1B3 as important regulators of the pharmacokinetics of substrate drugs. Biol Pharm Bull. 2015;38(2):155–68. https://doi.org/10.1248/bpb.b14-00767.
63. Mahmutefendić H, Zagorac GB, Maćešić S, Lučin P. Rapid endosomal recycling. Peripheral membrane proteins. 2018. https://www.intechopen.com/chapters/60064. https://doi.org/10.5772/intechopen.75685.
64. Au JL, Yeung BZ, Wientjes MG, Lu Z, Wientjes MG. Delivery of cancer therapeutics to extracellular and intracellular targets: determinants, barriers, challenges and opportunities. Adv Drug Deliv Rev. 2016;97:280–301. https://doi.org/10.1016/j.addr.2015.12.002.
65. Jung D, Hagenbuch B, Gresh L, Pontoglio M, Meier PJ, Kullak-Ublick GA. Characterization of the human OATP-C (SLC21A6) gene promoter and regulation of liver-specific

OATP genes by hepatocyte nuclear factor 1 alpha. J Biol Chem. 2001;276(40):37206–14. https://doi.org/10.1074/jbc.M103988200.
66. Yao J, Hong W, Huang J, Zhan K, Huang H, Hong M. N-glycosylation dictates proper processing of organic anion transporting polypeptide 1B1. PLoS ONE. 2012;7(12):e52563. https://doi.org/10.1371/journal.pone.0052563.
67. Murk JL, Stoorvogel W, Kleijmeer MJ, Geuze HJ. The plasticity of multivesicular bodies and the regulation of antigen presentation. Semin Cell Dev Biol. 2002;13(4):303–11. https://doi.org/10.1016/s1084952102000605.
68. Russell MR, Nickerson DP, Odorizzi G. Molecular mechanisms of late endosome morphology, identity and sorting. Curr Opin Cell Biol. 2006;18(4):422–8. https://doi.org/10.1016/j.ceb.2006.06.002.
69. Saksena S, Sun J, Chu T, Emr SD. ESCRTing proteins in the endocytic pathway. Trends Biochem Sci. 2007;32(12):561–73. https://doi.org/10.1016/j.tibs.2007.09.010.
70. van Meel E, Klumperman J. Imaging and imagination: understanding the endo-lysosomal system. Histochem Cell Biol. 2008;129(3):253–66. https://doi.org/10.1007/s00418-008-0384-0.
71. Williams RL, Urbe S. The emerging shape of the ESCRT machinery. Nat Rev Mol Cell Biol. 2007;8(5):355–68. https://doi.org/10.1038/nrm2162.
72. Jung D, Podvinec M, Meyer UA, Mangelsdorf DJ, Fried M, Meier PJ, *et al*. Human organic anion transporting polypeptide 8 promoter is transactivated by the farnesoid X receptor/bile acid receptor. Gastroenterology. 2002;122(7):1954–66.
73. Konig J, Cui Y, Nies AT, Keppler D. A novel human organic anion transporting polypeptide localized to the basolateral hepatocyte membrane. Am J Physiol Gastrointest Liver Physiol. 2000;278(1):G156–64.
74. Clarke JD, Novak P, Lake AD, Hardwick RN, Cherrington NJ. Impaired N-linked glycosylation of uptake and efflux transporters in human non-alcoholic fatty liver disease. Liver Int. 2017;37(7):1074–81. https://doi.org/10.1111/liv.13362.
75. Rothman S. How is the balance between protein synthesis and degradation achieved? Theor Biol Med Model. 2010;7:25. https://doi.org/10.1186/1742-4682-7-25.
76. Millward DJ, Bates PC, Rosochacki S. The extent and nature of protein degradation in the tissues during development. Reprod Nutr Dev. 1981;21(2):265–77. https://doi.org/10.1051/rnd:19810210.
77. Arias IM, Doyle D, Schimke RT. Studies on the synthesis and degradation of proteins of the endoplasmic reticulum of rat liver. J Biol Chem. 1969;244(12):3303–15.
78. Barle H, Nyberg B, Essen P, Andersson K, McNurlan MA, Wernerman J, *et al*. The synthesis rates of total liver protein and plasma albumin determined simultaneously in vivo in humans. Hepatology. 1997;25(1):154–8. https://doi.org/10.1002/hep.510250128.
79. Kimoto E, Yoshida K, Balogh LM, Bi YA, Maeda K, El-Kattan A, *et al*. Characterization of organic anion transporting polypeptide (OATP) expression and its functional contribution to the uptake of substrates in human hepatocytes. Mol Pharm. 2012;9(12):3535–42. https://doi.org/10.1021/mp300379q.
80. Varma MV, Lai Y, Feng B, Litchfield J, Goosen TC, Bergman A. Physiologically based modeling of pravastatin transporter-mediated hepatobiliary disposition and drug-drug interactions. Pharm Res. 2012;29(10):2860–73. https://doi.org/10.1007/s11095-012-0792-7.
81. Murray M, Zhou F. Trafficking and other regulatory mechanisms for organic anion transporting polypeptides and organic anion transporters that modulate cellular drug and xenobiotic influx and that are dysregulated in disease. Br J Pharmacol. 2017;174(13):1908–24. https://doi.org/10.1111/bph.13785.
82. Leonhardt M, Keiser M, Oswald S, Kuhn J, Jia J, Grube M, *et al*. Hepatic uptake of the magnetic resonance imaging contrast agent Gd-EOB-DTPA: role of human organic anion transporters. Drug Metab Dispos. 2010;38(7):1024–8. https://doi.org/10.1124/dmd.110.032862.
83. Sai Y, Kaneko Y, Ito S, Mitsuoka K, Kato Y, Tamai I, *et al*. Predominant contribution of organic anion transporting polypeptide OATP-B (OATP2B1) to apical uptake of estrone-3-sulfate by human intestinal Caco-2 cells. Drug Metab Dispos. 2006;34(8):1423–31. https://doi.org/10.1124/dmd.106.009530.
84. Huotari J, Helenius A. Endosome maturation. EMBO J. 2011;30(17):3481–500. https://doi.org/10.1038/emboj.2011.286.
85. Mateus A. Intracellular unbound drug concentrations. Methodology and application for understanding cellular drug exposure. Digital comprehensive summaries of Uppsala dissertations: Upsala, Sweden; 2016. https://uu.diva-portal.org/smash/get/diva2:908586/FULLTEXT01.pdf.
86. Eytan GD, Regev R, Oren G, Assaraf YG. The role of passive transbilayer drug movement in multidrug resistance and its modulation. J Biol Chem. 1996;271(22):12897–902. https://doi.org/10.1074/jbc.271.22.12897.
87. Mathieson T, Franken H, Kosinski J, Kurzawa N, Zinn N, Sweetman G, *et al*. Systematic analysis of protein turnover in primary cells. Nat Commun. 2018;9(1):689. https://doi.org/10.1038/s41467-018-03106-1.